Ecotoxicology and Environmental Safety 236 (2022) 113509

Contents lists available at ScienceDirect

Ecotoxicology and Environmental Safety

journal homepage: www.elsevier.com/locate/ecoenv

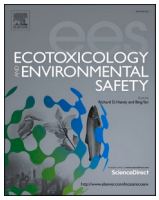

Adsorption of cadmium on clay-organic associations in different pH solutions: The effect of amphoteric organic matter

Wenpo Xu [a,b], Chengshuai Liu [b], Jian-Ming Zhu [c], Hongling Bu [a,*], Hui Tong [a], Manjia Chen [a,*], Decan Tan [b], Ting Gao [b], Yizhang Liu [b]

[a] National-Regional Joint Engineering Research Center for Soil Pollution Control and Remediation in South China, Guangdong Key Laboratory of Integrated Agro-environmental Pollution Control and Management, Institute of Eco-environmental and Soil Sciences, Guangdong Academy of Sciences, Guangzhou 510650, China
[b] State Key Laboratory of Environmental Geochemistry, Institute of Geochemistry, Chinese Academy of Sciences, Guiyang 550081, China
[c] State Key Laboratory of Geological Processes and Mineral Resources, China University of Geosciences, Beijing 100083, China

ARTICLE INFO

Edited by Dr. Hao Zhu

Keywords:
Cadmium
Montmorillonite
Clay-organic complexes
Adsorption
Amphoteric organic matter

ABSTRACT

Clay minerals are important soil components and usually coexist with organic matter, forming mineral-organic associations (MOAs), which control the speciation, mobility, and bioavailability of heavy metals. However, the adsorption mechanism of cadmium (Cd) by MOAs is still unclear, especially for the associations of amphoteric organic matter and clay minerals. In this study, 12-aminododecanoic acid (ALA) and montmorillonite (Mt) were chosen to prepare MOAs via intercalation (Mt-ALA composite) and physical mixing (Mt-ALA mixture). Batch experiments were conducted to investigate the adsorption mechanism of Cd(II) by MOAs under different pH values and initial Cd(II) concentrations. The results showed that the Cd(II) adsorption capacities followed as Mt > Mt-ALA mixture > Mt-ALA composite under acidic conditions, Mt-ALA mixture > Mt > Mt-ALA composite under neutral conditions, and Mt-ALA mixture > Mt-ALA composite > Mt under alkaline conditions, suggesting the adsorption behaviors of Cd(II) by MOAs were primarily constrained by the speciation of ALA and solution pH. Under acidic conditions, cationic $HALA^+$ could intercalate into the interlayer of Mt and occupy the adsorption sites, reducing the adsorption capacity of Cd(II). As pH increased to neutral, $HALA^+$ decreased and changed to a zwitterionic state, which caused ALA to release out from the interlayer of Mt-ALA composite or not easily enter into Mt-ALA mixture and promoted Cd(II) adsorption. Under alkaline conditions, the increase of anion ALA^- would cause ALA to be mainly adsorbed on the surface of Mt and chelate with Cd(II), enhancing the adsorption of Cd(II). Further analysis by Fourier transform infrared and X-ray photoelectron spectroscopy indicated that the carboxyl and amino groups of ALA both participated in the adsorption of Cd(II). These findings could extend the knowledge on the mobility and fate of Cd in clay-based soils and be used as a basis for understanding the biogeochemical behavior of Cd in the environment.

1. Introduction

Cadmium (Cd) is a global toxic pollutant due to its long-range transport, persistence, and biological accumulation in the environment (Nriagu, 1990). In recent years, Cd pollution in soils has become extremely serious with the intensification of anthropogenic activities such as industrial discharge, nonferrous metal mining and smelting, fossil fuel combustion, and excessive usage of agricultural fertilizer (Nriagu, 1990; Liu et al., 2021). Soil Cd contamination poses a great threat to living organisms and humans (Satarug et al., 2003; Yang et al., 2018). Generally, the aqueous concentration and migration of Cd in the subsurface highly depend on its adsorption and desorption behaviors in soils (Naidu et al., 1997; Mo et al., 2021; Zhu et al., 2022).

Clay minerals are important components of soils. Owing to their high cation exchange capacity (CEC), large specific surface area and surface charges, clay minerals can strongly adsorb metal ions and plays a significant role in constraining the mobility and bioavailability of heavy metals in clay-based soils, sediments, and suspended particles (Brigatti et al., 2006; Du et al., 2017). Nonetheless, previous studies have indicated that individual soil components, including clay minerals, do not exist alone in soils, and they often combine with other components (e.g., inorganic or organic) to form binary or multivariate (i.e., ternary)

* Corresponding authors.
E-mail addresses: hlbu@soil.gd.cn (H. Bu), mjchen@soil.gd.cn (M. Chen).

https://doi.org/10.1016/j.ecoenv.2022.113509
Received 24 January 2022; Received in revised form 31 March 2022; Accepted 8 April 2022
Available online 11 April 2022

complexes (Theng et al., 2008; Du et al., 2016c), such as binary clay-bacteria and clay-humic acid (HA) composites, and ternary clay-HA-bacteria composite (Du et al., 2016a). Therefore, these combinations influence the relationships of individual components with the surrounding environment. For instance, the combination of ferric (hydr) oxides and clay minerals can affect the adsorption of heavy metals by clay minerals (Landry et al., 2009). Furthermore, some natural polar OM tends to complex with clay minerals and plays an important role in the fate of heavy metals (Zhu et al., 2016; de Oliveira et al., 2021). The primary reason is that OM contains various functional groups, such as carboxylic and phenolic groups (Van Riemsdijk et al., 2006). These functional groups could change the physicochemical properties of the mineral surface (e.g., adsorption characteristics) and act as carriers to complex with metal ions, which promotes the formation of organic metal chelates and enhances the adsorption capacity of clay minerals (Du et al., 2016a; Zhu et al., 2019).

However, the interaction between clay minerals and OM is even more complicated. It has been demonstrated that the active sites of clay minerals include silanol sites (Si-OH), aluminol sites (Al-OH), intercalated exchangeable cations, and isomorphic replacement sites (Fan et al., 2014). These active sites allow clay minerals to bind with OM in a variety of pathways, such as ligand exchange, surface complexation, multivalent ion bond bridging (e.g., water bridging between organic molecules and hydrated cations), weak interaction forces (e.g., hydrophobic, van der Waals and hydrogen bonds), cation exchange, electrostatic adsorption, and cation-π interactions (Lagaly et al., 2013; Du et al., 2016a, 2017; Zhu et al., 2016). Moreover, it is worth noting that some organics can intercalate into the interlayer space of swelling clay minerals to form interlayer clay-organic composites through cation-exchange reactions in which organic guests replace the original hydrated cations (Theng et al., 2008; Bu et al., 2019b). Indeed, interlayer clay-organic composites are widely found in soils or sediments (Lagaly et al., 2013). The interlayer distances of swelling clay minerals would increase due to the intercalated OM (Yuan et al., 2013; Bu et al., 2017), affecting the adsorption behavior of ions. One of the possibilities is that the increased interlayer distance could provide more space for the adsorption of heavy metals (Zhu et al., 2019). Alternatively, OM entering the interlayer may block interlayer pores or occupy adsorption sites, decreasing the adsorption capacity of heavy metals (Du et al., 2016b; Zhou et al., 2017). Actually, it's far from it. The adsorption of heavy metals onto interlayer clay-organic complex also depends on the types of swelling clay minerals and OM as well as the surrounding environment.

Amino acids (AAs) are not only one of the basic substances of living organisms but also a significant component of OM in the nonliving matter, such as sediment, soil, fossils, and water (Parbhakar et al., 2007; Theng et al., 2008; Rothstein, 2010). They are often associated with minerals (e.g., clay minerals, hydroxyl iron oxides, and silica) via sorption or intercalating (Kitadai et al., 2009; Zhu et al., 2016), forming mineral-organic associations (MOAs) that affect the biogeochemistry cycle of heavy metals. Many researchers have investigated the interaction between AAs and minerals and heavy metals. Compared with the raw clay minerals, MOAs that formed with AAs have a higher adsorption capacity for heavy metals (Brigatti et al., 2003; El Adraa et al., 2017; Zhu et al., 2019). For example, Brigatti et al. (2003) observed that glycine and cysteine enhanced the retention abilities of beidellite for Cu(II) in solution with pH 5.5. In these studies, however, there are only a few researches about Cd(II) adsorption by the clay minerals associated with AAs (El Adraa et al., 2017). Moreover, information about the combination mode between AAs and clay minerals has either been neglected or has received very little attention, resulting in the adsorption mechanisms of Cd(II) to MOAs are not well understood. In particular, it remains unclear that how the structure and surface properties of clay-organic composites affect the adsorption of Cd(II) under different pH values.

In this study, MOAs, including clay-AAs composite and clay-AAs mixture, were prepared and used for Cd(II) adsorption experiment. Montmorillonite, a representative clay mineral, was selected due to its prevalence and swelling property, which enables the intercalation of OM (Liu et al., 2013; Du et al., 2016a). 12-aminododecanoic acid (ALA, $NH_2(CH_2)_{10}CH_2COOH$) was selected as: (1) ALA is a moderate-chainamphoteric OM containing carboxyl and amino groups, and (2) ALA can intercalate into the interlayer of Mt through cation exchange when protonated (Yuan et al., 2013; Bu et al., 2019a), which leads to a large interlayer distance that may be convenient for investigating the interaction between heavy metal ions and the interlayer structure of Mt. Based on the results of X-ray diffraction (XRD), Fourier transform infrared (FT-IR) spectroscopy, and X-ray photoelectron spectroscopy (XPS), this study investigated the effect of the interlayer structure and functional groups of MOAs on Cd(II) adsorption under different pH conditions and discussed the adsorption mechanism. The results of this study are expected to improve the understanding of the mechanisms of migration, transformation, and immobilization of Cd(II) in soils, sediments, and water.

2. Materials and methods

2.1. Materials

The Mt sample in this study was obtained from Inner Mongolia, China. The raw Mt was treated with a precipitation purification method to obtain < 2 μm particles for adsorption experiments. According to the results of XRD analysis, Mt did not contain any other minerals except for minor quartz (>97% purity). The structural formula of Mt is: $Ca_{0.168}Na_{0.025}K_{0.013}[Si_{3.984}Al_{0.016}[Al_{1.352}Fe_{0.271}Mg_{0.365}Ti_{0.010}]O_{10}(OH)_2{\cdot}nH_2O$ (Yuan et al., 2013). The CEC of Mt was 110.5 mmol/100 g and the Brunauer-Emmett-Teller (BET) specific surface area of Mt was 57.3 m^2/g (Bu et al., 2017). ALA was purchased from Sigma Aldrich (>98% purity), and $Cd(NO_3)_2{\cdot}4\ H_2O$ was purchased from Alfa Aesar (>99.99% purity). All chemicals were analytical grade and used without further purification. Milli-Q water (18.2 mΩ·cm) was used for preparing solutions and washing samples.

2.2. Preparation of MOAs

Two kinds of MOAs were prepared: Mt-ALA composite and Mt-ALA mixture. Mt-ALA composite was prepared mainly through the cation exchange method, namely, by making the cationic groups ($-NH_3^+$) of ALA exchange with the interlayer cations (Na^+, Ca^{2+}, etc.) of Mt (Zhu et al., 2016). To optimize the exchange effect, Mt was treated with 0.5 mol/L NaCl solution before preparing the composite, as detailed in Bu et al., (2017, 2019a). Mt-ALA mixture was prepated by mechanical mixing. For convenience, the raw Mt was denoted as Mt, while the prepared cation-exchanged sample with sodium was denoted as Na-Mt.

The detailed preparation procedure of the MOAs was as follows: for the preparation of the Mt-ALA composite, 22.1 mmol ALA (2.0 CEC) was first added to 200 mL 0.14 mol/L HCl solution and placed in an 80 °C water bath. Then, the solution was slowly added into a mixture of 10.0 g Na-Mt and 1000 mL MQ water. After stirring at 80 °C for 30 min, the suspension was centrifuged (7200 g), and the solid was repeatedly washed with large amounts of 60 °C MQ water to remove the excessive ALA and Cl^- until the filtrate was free of Cl^- (tested with $AgNO_3$ solution), and then freeze-dried and ground into powder (Yuan et al., 2013; Bu et al., 2019a). The prepared sample was labeled as Mt-ALA composite ($Na\text{-}Mt\text{-}ALA_{inter}$). The elemental analysis showed that the content of ALA in Mt-ALA composite was 19.0 wt%, which was performed using an Elementar Vario EL III Universal CHNOS elemental analyzer. For the preparation of the Mt-ALA mixture, 4.0 g Na-Mt sample and 1.0 g ALA were mechanically mixed by grinding for 10 min under the natural condition (Bu et al., 2019a). The prepared sample was labeled as $Na\text{-}Mt\text{-}ALA_{mix}$. The content of ALA in MOAs was 20.0 wt%.

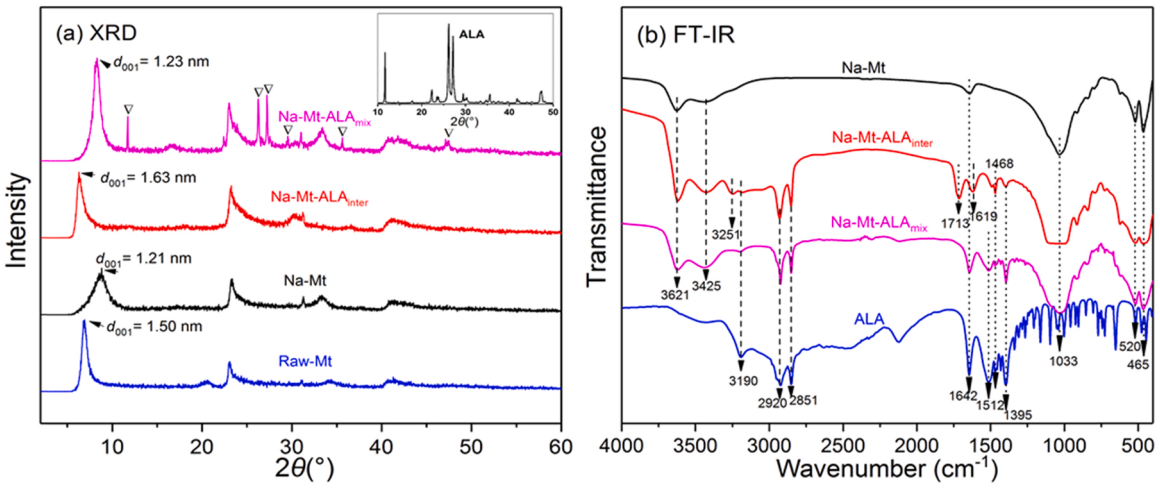

Fig. 1. The characterization of raw montmorillonite (Raw-Mt), Na-montmorillonite (Na-Mt), 12-aminododecanoic acid (ALA), and the associations of Na-montmorillonite and 12-aminododecanoic acid (Na-Mt-ALA$_{inter}$ and Na-Mt-ALA$_{mix}$). (a) X-ray diffraction patterns (XRD, 2–60°), ∇ represents ALA. (b) Fourier transform infrared spectroscopy (FT-IR, 4000–400 cm^{-1}).

2.3. Characterization of samples

XRD patterns were recorded on a Bruker D2 Advance diffractometer with Co-Kα radiation (λ = 0.179 nm), using a generator voltage of 36 kV, a generator current of 36 mA, a step size of 0.02° (2θ) and a scanning speed of 0.2 s per step (scanning range 2–80°). FT-IR spectra of the samples were measured on a Bruker Vertex-70 FTIR spectrometer. The KBr pressed pellet method was used for the FT-IR analysis, and the spectra were collected over a range of 400–4000 cm^{-1} with 64 scans at a resolution of 4 cm^{-1}. In this study, approximately 0.9 mg sample and 80 mg KBr were used for analysis (Bu et al., 2019a). XPS analyses were carried out on a Thermo Scientific K-Alpha spectrometer equipped with an Al Kα source. The spectra were collected with a pass energy of 30 eV and an analysis area of 400 μm^2. All spectra were obtained with smart background correction (Ma et al., 2015).

2.4. Adsorption experiments

2.75 g $Cd(NO_3)_2{\cdot}4\ H_2O$ solid was dissolved in 100 mL MQ water to prepare a 10,000 mg/L stock solution. Batch experiments were carried out to study the adsorption capacities of Mt and MOAs in aqueous solutions. In this experiment, the solid-liquid ratio was fixed at 1.0 g/L, the pH of the suspension was 3, 5, 7, and 9, and the initial Cd(II) concentration was 1.0–100 mg/L. First, 50 mg adsorbent was added into a centrifuge tube with 0.001 mol/L $NaNO_3$ solutions, and the volume of final suspension was 50 mL after adjusting pH with 0.1 mol/L HNO_3 or NaOH solution. The suspensions were shaken using a rotary shaker at 150 r/min for 24 h, and the pH was readjusted. Then, the suspensions were divided into 15 mL centrifuge tubes, and a certain amount of Cd(II) solution was added to make a Cd(II) concentration varying from 1.0 mg/L to 100 mg/L, after which the tubes were shaken (150 r/min) at room temperature (22 ± 2 °C). A 24 h duration was chosen for Cd(II) adsorption experiments to reach equilibrium according to the kinetics results of a preliminary experiment (Fig. S1). After equilibration, the suspensions were centrifuged at 10,000 g for 10 min. The supernatants were subsequently filtered through 0.22-μm polysulfone membranes into centrifuge tubes, and the solids were freeze-dried and ground to 200 mesh using an agate mortar for characterization (e.g., XRD, XPS, and FT-IR). In addition, control experiments without Cd(II) addition were set up to compare the effect of pH on the structure and morphology of the adsorbents. All adsorption experiments were conducted at least in duplicate.

The concentration of Cd(II) in the solution was measured with inductively coupled plasma atomic emission spectrometry (ICP-OES). The amount of Cd(II) adsorbed per unit mass of adsorbent (Q_e) was calculated according to Eq. (1):

$$Q_e = (C_0 - C_e) \times V/m \quad (1)$$

where Q_e is the adsorption capacity (mg/g), C_0 and C_e are the initial and equilibrium concentrations of Cd(II) (mg/L), respectively, V is the volume of solution (L), and m is the weight of adsorbent (g).

To further characterize the adsorption process of Cd(II) by MOAs, the Langmuir and Freundlich isotherm models were used to fit the adsorbed data. The Langmuir and Freundlich isotherm models are shown in Eqs. (2) and (3), respectively:

$$C_e/Q_e = 1/(Q_m \times K_L) + C_e/Q_m \quad (2)$$

$$\ln(Q_e) = \ln(K_F) + \ln(C_e)/n \quad (3)$$

where Q_m is the maximum adsorption amount (mg/g), K_L is the Langmuir constant (L/mg). K_F is the Freundlich constant ((mg/g)(L/mg)$^{1/n}$), n is a dimensionless coefficient depicting the adsorption intensity (Xu et al., 2021).

3. Results and discussion

3.1. Characterization of samples

The XRD patterns of Mt, ALA, and MOAs are shown in Fig. 1a. For raw Mt (Ca-Mt), the value of d_{001} was 1.50 nm. After sodium treatment, the value of d_{001} decreased to 1.21 nm. The d_{001} values of the Mt-ALA mixtures increased slightly from 1.21 nm to 1.23 nm. Previous studies pointed out that the interlayer distance varied with the nature of the interlayer cations and the amount of available water or other polar molecules (Brigatti et al., 2006; de Oliveira et al., 2021). Thus, these XRD results showed that the mechanical mixing of ALA and Mt made some ALA enter into the interlayer of Mt, but the amount was very limited. Moreover, the characteristic peak positions of ALA (11.6°, 26.2°, 27.2°, and 47.4°) and Mt (7.6°, 23.3°, and 41.4°) were exhibited in the XRD patterns of the mixtures, indicating that ALA was mainly adsorbed on the outside of the interlayer structure of Mt (Liu et al., 2013; Yuan et al., 2013). For the Na-Mt-ALA composite, the d_{001} value was 1.63 nm, larger than that of Na-Mt (1.21 nm). This result suggested that the interlayer distance was approximately 0.67 nm, which was obtained by subtracting the thickness of the tetrahedron-octahedron-tetrahedron layer (0.96 nm, Lagaly et al., 2013). The interlayer distance of

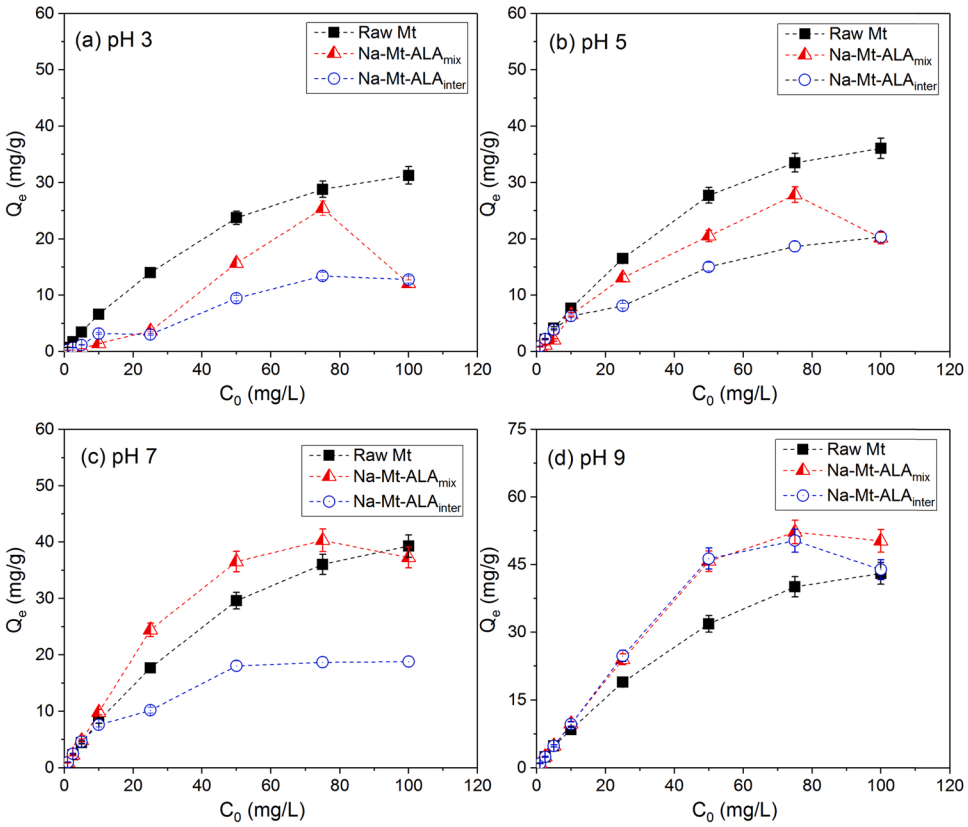

Fig. 2. The adsorption capacities of Cd(II) by the Raw-Mt, Na-Mt-ALA mixture (Na-Mt-ALA-$_{mix}$), and Na-Mt-ALA composite (Na-Mt-ALA$_{inter}$) under different pH conditions (adsorbent dosage = 1.0 g/L, $C_{0,\ Cd}$ = 0–100 mg/L, ionic strength = 0.001 mol/L $NaNO_3$, temperature = 22 ± 2 °C, Time = 24 h). (a) pH 3, (b) pH 5, (c) pH 7, (d) pH 9. Solid squares represent Raw Mt, half-solid triangles represent Na-Mt-ALA$_{mix}$, open circles represent Na-Mt-ALA$_{inter}$. Error bars show the standard errors from triplicate measurements.

Na-Mt-ALA composite was larger than that of Na-Mt (approximately 0.25 nm), indicating the intercalation of ALA within the interlayer space of Mt (Yuan et al., 2013; Bu et al., 2019a). Although the (001) diffraction (6.3°) of Na-Mt-ALA composite shifted toward a low angle compared to that of Na-Mt, the structure of Mt in the MOAs was not destroyed.

The FT-IR spectra of the MOAs showed the characteristic bands of Mt and ALA, such as the anti-symmetric (2920 cm^{-1}) and symmetric stretching vibration peaks (2851 cm^{-1}) of -CH_2 and the symmetric stretching vibration peak (1395 cm^{-1}) of R-COO^- (Fig. 1b), confirming the presence of ALA (Bu et al., 2019a). However, the structural hydroxyl stretching vibration band (3621 cm^{-1}) and water OH band (3425 cm^{-1}) of Mt decreased significantly. For the Mt-ALA composite (Na-Mt-A-LA$_{inter}$), the band positions of interlayer water and adsorbed water of Mt changed significantly, shifting from 1642 cm^{-1} to 1619 cm^{-1}. In addition, the characteristic infrared band of ALA in the Mt-ALA composite was different from that of pure ALA. This difference was due to the protonation of functional groups of ALA with the addition of hydrochloric acid in the intercalation process, e.g., the amino groups of ALA intercalated into the interlayer and became -NH_3^+ (such as the band at 3251 cm^{-1}) (Stathi et al., 2007; Bu et al., 2019a).

3.2. Cd(II) adsorption by MOAs

The adsorption experiments of Cd(II) by Mt and the MOAs were conducted as a function of pH and Cd concentration. As shown in Fig. 2, the adsorption capacity of Cd(II) by Mt increased from 31.43 mg/g to 43.25 mg/g within the pH range from 3.0 to 9.0. The pH dependence of Cd(II) adsorption by Mt could be ascribed to the number of available exchange sites for Cd(II) (Fan et al., 2014; Gu et al., 2010). With increasing pH, especially under alkaline conditions, the silanol and aluminol groups at the edge sites would carry more negative charges due to the dissociation of ≡SOH to form ≡SO^- (Gu et al., 2010). These

Table 1
Langmuir and Freundlich model parameters of Cd(II) adsorption by Raw-Mt, Na-Mt-ALA composite (Na-Mt-ALA$_{inter}$), and Na-Mt-ALA mixture (Na-Mt-ALA$_{mix}$) under different pH conditions (adsorbent dosage = 1.0 g/L, $C_{0,\ Cd}$ = 0–100 mg/L, ionic strength = 0.001 mol/L $NaNO_3$, temperature = 22 ± 2 °C, Time = 24 h).

		Langmuir model			Freundlich model		
	pH	Q_m (mg/g)	k_L (L/mg)	R^2	k_f ((mg/g)(L/mg)$^{1/n}$)	n	R^2
Raw Mt	3	38.31 ± 0.87	0.063	0.997	2.282	1.46 ± 0.08	0.980
	5	39.84 ± 1.64	0.128	0.990	4.154	1.72 ± 0.07	0.988
	7	40.98 ± 1.99	0.180	0.986	5.478	1.90 ± 0.09	0.988
	9	45.05 ± 2.55	0.241	0.980	5.448	2.13 ± 0.21	0.984
Na-Mt-ALA$_{inter}$	3	13.70 ± 5.75	0.014	0.482	0.428	1.26 ± 0.08	0.958
	5	19.34 ± 2.27	0.316	0.980	3.487	2.52 ± 0.11	0.987
	7	21.14 ± 1.08	0.116	0.926	5.779	3.52 ± 0.25	0.968
	9	45.45 ± 1.28	1.560	0.995	12.67	2.10 ± 0.36	0.761
Na-Mt-ALA$_{mix}$	3	–	-0.003	0.040	0.146	0.88 ± 0.09	0.927
	5	22.78 ± 2.26	0.236	0.943	3.611	2.04 ± 0.26	0.900
	7	39.22 ± 1.25	0.600	0.993	8.995	2.23 ± 0.42	0.681
	9	52.36 ± 0.91	0.770	0.998	11.867	1.87 ± 0.27	0.857

Note: - represents not shown because the value was negative, which is abnormal.

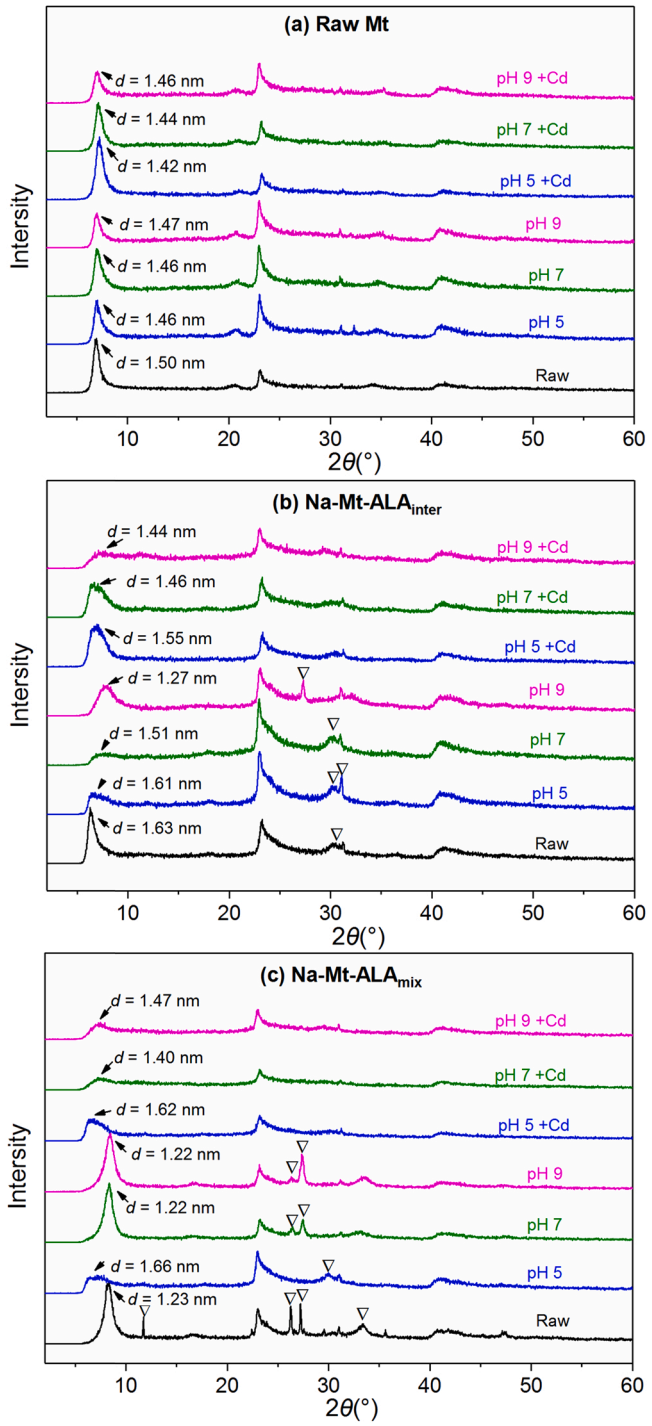

Fig. 3. XRD results of acid-base treated Mt and Na-Mt-ALA complexes (labeled as pH 5, pH 7, and pH 9), and Mt and Na-Mt-ALA complexes after Cd(II) adsorption at different pH values (labeled as pH 5 + Cd, pH 7 + Cd, and pH 9 + Cd; adsorbent dosage = 1.0 g/L, $C_{0,\ Cd}$ = 75 mg/L, Time = 24 h). All *d* values show the values of 001 reflection, ▽ represents ALA. (a) Raw Mt, (b) Na-Mt-ALA composite (Na-Mt-ALA$_{inter}$), and (c) Na-Mt-ALA mixture (Na-Mt-ALA$_{mix}$).

changes in surface charge could cause an increase in Cd(II) adsorption.

In contrast, the adsorption capacities of Cd(II) by MOAs were related to solution pH and the types of MOAs (i.e., composite and mixture). Under acidic conditions (pH 3 and 5), the Cd(II) adsorption capacities were 13.90 mg/g and 21.16 mg/g for Na-Mt-ALA$_{inter}$, 18.45 mg/g and 24.73 mg/g for Na-Mt-ALA$_{mix}$, respectively, less than that of Mt (31.43 mg/g and 35.44 mg/g, respectively) (Fig. 2). This result was possibly due to the presence of ALA occupying some adsorption sites (Brigatti et al., 2003; El Adraa et al., 2017; Zhou et al., 2017), inhibiting the adsorption of Cd(II). Under neutral conditions, however, the adsorption capacity of Cd(II) by the Na-Mt-ALA$_{mix}$ (41.24 mg/g) was higher than that of raw Mt (38.71 mg/g). In comparison, the adsorption capacity of Cd(II) by Na-Mt-ALA$_{inter}$ (19.92 mg/g) was lower than that of raw Mt. Under alkaline conditions (pH 9), the Cd(II) adsorption capacities of all MOAs (52.91 mg/g and 50.21 mg/g, respectively) were much higher than that of raw Mt (43.25 mg/g). This phenomenon was related to the decrease in the "blocking effects" of OM with increasing pH (Fan et al., 2014), resulting in the functional groups of ALA adsorbed on Mt could be readily reacted with Cd(II). In addition, the Cd(II) adsorption capacity of Na-Mt-ALA$_{inter}$ at pH 9 was still lower than that of Na-Mt-ALA$_{mix}$, which may be due to that some ALA existed in the interlayer space of Na-Mt-ALA$_{inter}$ did not release out and occupied the interlayer adoption sites.

3.3. Adsorption isotherms

The simulated linear figures and associated parameters for Mt and MOAs are presented in Table 1 and Fig (S2 and S3), respectively. It was found that the adsorption of Cd(II) by Mt alone could be better described by the Langmuir model at pH < 7 while by the Freundlich model at pH > 7, indicating that the Cd adsorption was mainly controlled by one type of adsorption site at lower pH and multilayer adsorption sites at higher pH, respectively. In contrast, adsorption of Cd(II) by the MOAs (including Na-Mt-ALA$_{inter}$ and Na-Mt-ALA$_{mix}$) could be better described by the Freundlich model at pH < 7 while by the Langmuir model at pH > 7. These results suggested that, for MOAs, heterogeneous adsorption played an important role under acidic conditions, while homogeneous adsorption mainly occurred under basic conditions.

The calculated maximum adsorption amount ranking from high to low is Mt, Na-Mt-ALA$_{mix}$, and Na-Mt-ALA$_{inter}$ at acidic and neutral conditions (Table 1). It should be pointed out that the calculated maximum adsorption amount of Na-Mt-ALA$_{inter}$ and Na-Mt-ALA$_{mix}$ at pH 9 was greater than that of Mt. The calculated maximum adsorption amount of Na-Mt-ALA$_{mix}$ ranked the first among the three samples at basic condition. The actual adsorption capacities of these samples were basically consistent with the calculated results. This phenomenon suggests that MOAs contains more metals binding sites at basic conditions. In addition, Temkin and Dubinin-Radushkevich isotherm models were used to understand the free energy of adsorption and the type of interaction that occurred during the adsorption process (Figs. S4 and S5, Table S1), the results showed that the mean sorption energy (E) were less than 8 kJ/mol, indicating that the adsorption was mainly a physical process (Chabani et al., 2006; Xu et al., 2022).

3.4. Effect of the interlayer structure of MOAs on Cd(II) adsorption

XRD analysis was performed with the Mt and MOAs at the corresponding pH through an acid and base treatment to investigate the microstructure of MOAs before Cd adsorption at different pH conditions. Then, the XRD analysis was also performed with the Mt and MOAs after Cd adsorption for 24 h (Fig. 3). The changes of interlayer structure of MOAs before and after Cd(II) adsorption were compared by XRD patterns. For raw Mt, the d_{001} values were almost unaffected by acid-base treatment but slightly decreased after Cd(II) adsorption (Fig. 3a). This phenomenon implied that Cd(II) may enter the interlayer space of Mt by exchange with interlayer cation Ca^{2+}, for that the hydration radius of Ca is larger than that of Cd (Mobasherpour et al., 2012).

Likewise, a difference in d_{001} values was observed in the case of MOAs before and after Cd(II) adsorption at different pH values in the XRD patterns (Fig. 3b and c). For Na-Mt-ALA$_{inter}$, the d_{001} values decreased from 1.63 nm to 1.27 nm with increasing pH before Cd(II) adsorption (Fig. 3b). This result indicated that ALA mainly occurred in the interlayer space of Na-Mt-ALA$_{inter}$ at pH 5 and 7 but little remained

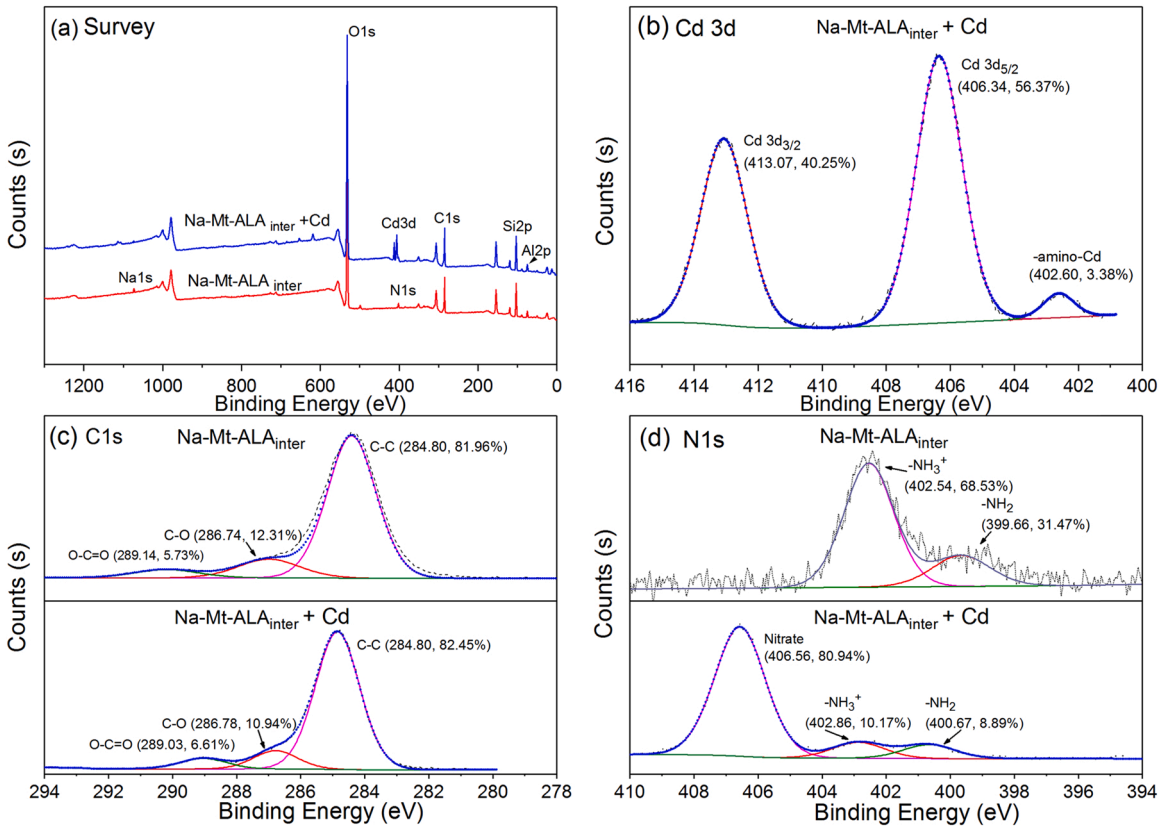

Fig. 4. The XPS spectrum of Na-Mt-ALA composite (Na-Mt-ALA_{inter}) before and after Cd adsorption at pH 9 (adsorbent dosage = 1.0 g/L, $C_{0,\ Cd}$ = 75 mg/L, Time = 24 h): Full spectrum (a), Cd3d spectrum (b), C1s spectrum (c), and N1s spectrum (d).

in the interlayer at pH 9 (1.27 nm > 1.21 nm) (Bu et al., 2019a). After Cd(II) adsorption, the d_{001} values of the samples decreased at pH 5 and 7 but increased at pH 9. This suggested that Cd(II) may enter the interlayer space by exchange with organic compounds containing -NH_3^+ at pH 5 and 7 while with Na^+ at pH 9 (Zhu et al., 2016; El Adraa et al., 2017).

For Na-Mt-ALA_{mix}, the d_{001} value was 1.23 nm (Fig. 3c) which similar to that of sodium treatment Mt (Na-Mt, 1.21 nm), suggesting that ALA could not easily enter the interlayer of Mt without an acid and basic treatment. This is because the interlayer distance would be changed if the interlayer cations of Mt were replaced (Brigatti et al., 2013). Interestingly, the d_{001} of Na-Mt-ALA_{mix} increased to 1.66 nm at pH 5 before adsorption, which was approximately consistent with the result for Na-Mt-ALA (1.63 nm), while the d_{001} values were almost the same at pH 7 and 9 (Fig. 3c). These results suggested that ALA was protonated and entered into the interlayer space of Mt at pH 5. After Cd(II) adsorption, the d_{001} value of Na-Mt-ALA_{mix} slightly decreased, and the ALA characteristic peaks at 30° disappeared, implying that ALA participated in the Cd adsorption reaction at this pH. In contrast, the d_{001} value of Na-Mt-ALA_{mix} increased at pH 7 and 9 after adsorption, suggesting that Cd (II) entered the interlayer space of Mt by forming a bridge with Cd(II) under neutral and basic conditions (Stathi et al., 2007; Yan et al., 2019). In addition, it was not difficult to find that some characteristic peaks of ALA at 11.6° disappeared at pH 7and 9 before Cd adsorption (Fig. 3c), implying that parts of ALA outside the interlayer space of Mt were dissolved or some new substances were produced. After Cd adsorption, the ALA characteristic peaks further disappeared, suggesting that ALA adsorbed on the surface of Mt also participated in the adsorption reaction of Cd under neutral and basic conditions.

3.5. Effect of functional groups of MOAs on Cd(II) adsorption

To further explore the adsorption mechanism, XPS analysis was carried out to determine the changes of surface binding groups of MOAs before and after Cd(II) adsorption. The XPS results were analyzed by Gaussian fitting technology, and the analysis of C1s, N1s, and Cd3d XPS spectra of Na-Mt-ALA_{inter} and Na-Mt-ALA_{mix} before and after Cd(II) adsorption are summarized in Table S2. The XPS spectra of Na-Mt-ALA_{inter} before and after Cd(II) adsorption at pH 9 were taken as an example (Fig. 4). Three Cd 3d peaks at 402.60, 406.34, and 413.07 eV were observed for the Na-Mt-ALA_{inter} after Cd(II) adsorption (Fig. 4b). Especially, the strong peak at 406.34 eV could correspond to CdO or Cd $(OH)_2$, suggesting that Cd(II) was adsorbed by Na-Mt-ALA_{inter} through complexation with hydroxyl groups (-OH) or their deprotonated form (O^-) (Teng et al., 2020), which was also confirmed by the species of Cd at different pH values (Fig. S6). In addition, the peak at 402.60 eV was attributed to Cd(II) being bound to amide groups to form -N:-Cd^{2+} ($[Cd(NH_3)_6]^{2+}$) (Guo et al., 2017). These results indicated that Cd(II) ions could be complexed with the negative surface binding sites and the active amide groups of Na-Mt-ALA_{inter}.

Carbon is one of the main elements in ALA, and the C1s high-resolution spectra are presented in Fig. 4c. The carbon spectrum of ALA could be de-convoluted into three components at 284.80 eV, 286.74 eV, and 289.14 eV, corresponding to C-C in aliphatic or amino acid side chains, C-O/C-N in amine groups, and O═C-O in carboxyl groups, respectively (Yan et al., 2019). After Cd(II) adsorption, the binding energies of C-O and O-C═O changed, as well as the atomic ratios, suggesting that C-O and O-C═O participated in Cd(II) adsorption (Guo et al., 2017). The role of C- and O-containing groups in Cd(II) adsorption in this study may be described by the following reaction (Das et al., 2007; Du et al., 2017).

$$R\text{-}COO^- + Cd^{2+} \rightarrow R\text{-}COOCd \quad (4)$$

The high-resolution spectra of N1s have changed before and after Cd (II) adsorption presented in Fig. 4d. Before adsorption, N mainly existed

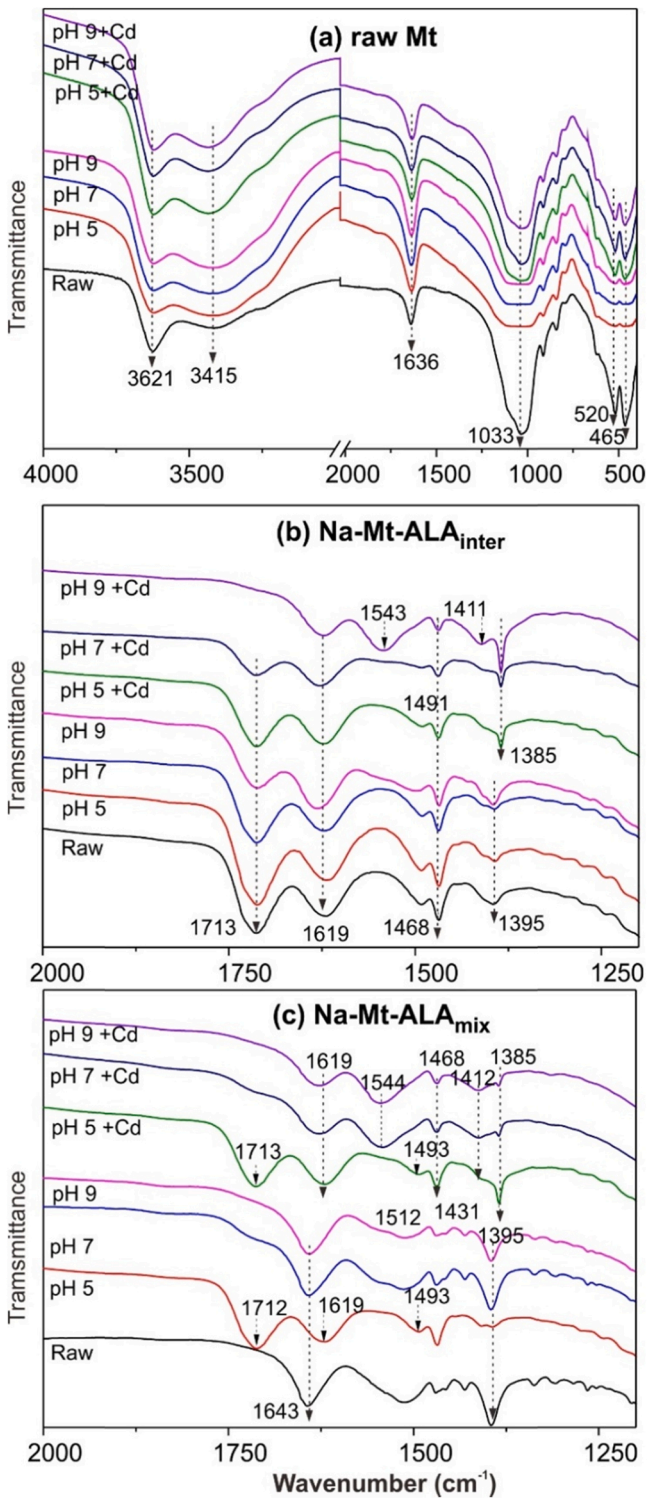

Fig. 5. FT-IR spectra of acid-base treated Mt and Na-Mt-ALA complexes (labeled as pH 5, pH 7, and pH 9), and Mt and Na-Mt-ALA complexes after Cd (II) adsorption at different pH values (labeled as pH 5 + Cd, pH 7 + Cd, and pH 9 + Cd; adsorbent dosage = 1.0 g/L, $C_{0,\ Cd}$ = 75 mg/L, Time = 24 h). (a) raw Mt (4000–400 cm^{-1}), (b) Na-Mt-ALA composite (Na-Mt-ALA$_{inter}$, 2000–1200 cm^{-1}), and (c) Na-Mt-ALA mixture (Na-Mt-ALA$_{mix}$, 2000–1200 cm^{-1}).

in the form of protonated R-NH_3^+ (402.54 eV), and the remaining N existed in non-protonated form as R-NH_2/R_2-NH (399.66 eV). After Cd (II) adsorption, a new peak at 406.56 eV appeared, corresponding to NO_3^- species. In addition, a new peak at 400.67 eV appeared, which resulted from lone pairs of electrons in the N atom that was bound by Cd (II) during the formation of the -N:-Cd^{2+} complex (Yan et al., 2019). This phenomenon indicated that the N-containing groups were involved in the adsorption of Cd(II). Similarly, Guo et al. (2017) also observed a strong peak at 405.28 eV when biomass-derived carbon sorbents were used to adsorb Cd(II). The role of N-containing groups in Cd(II) adsorption may be described by the following reactions (Yan et al., 2019):

$$R\text{-}NH_2 + Cd^{2+} \rightarrow R\text{-}NH_2Cd \quad (5)$$

$$R\text{-}NH_3^+ + Cd^{2+} \rightarrow R\text{-}NH_2Cd + H^+ \quad (6)$$

Meanwhile, we observed the changes of C 1 s, N 1 s, and Cd 3d XPS spectra for other samples for different pH conditions (Table S2). For both Na-Mt-ALA$_{mix}$ and Na-Mt-ALA$_{inter}$, it was noteworthy that big changes were found for N 1 s XPS spectra peaks. Except for the nitrate species (406.16 eV) that formed, it was observed that atomic ratios for the N peak that corresponded to R-NH_3^+ (402.33 eV) was significantly decreased after Cd(II) adsorption. This change showed the possibility of forming Cd in amino-Cd complexes. Similarly, the C atom in C-O or O═C-N could also strongly react with Cd(II), for the binding energy decreased after binding Cd(II).

In addition, FT-IR analysis was also used to investigate the changes of functional groups for MOAs before and after Cd adsorption. From the FT-IR spectra of Mt, the intensity of the OH stretching of water in Mt (3415 cm^{-1}) decreased after Cd(II) adsorption (Fig. 5a). This result showed that the interlayer water or adsorbed water of Mt was reduced after Cd(II) adsorption, suggesting that Cd is poorly hydrated replaced the interlayer calcium ions. These results also are consistent with the XRD analysis. The band at 1033 cm^{-1} was attributed to the stretching vibration of Si-O of the tetrahedral sheet (Bu et al., 2017, 2019a). Before Cd(II) adsorption, the bands for Mt at varying pH values were broad, but they became sharp after Cd(II) adsorption. The same phenomenon was exhibited in the bands at 520 and 465 cm^{-1}, which was attributed to the Si-O-Al deformation and Si-O-Si bending vibration of Mt, respectively. These differences in Si-O stretching vibrations may indicate that Si-O bonds participated in the adsorption of Cd(II) (Ma et al., 2010), namely, a small amount of Cd on Si-O group could evidently affect the Si-O-Al deformation and Si-O-Si bending vibration.

For Na-Mt-ALA$_{inter}$ before adsorption, except for the characteristic bands of ALA, the band positions of interlayer water and adsorbed water of Mt changed significantly, shifting from 1642 cm^{-1} to 1619 cm^{-1} (Fig. 1b). After Cd(II) adsorption, obvious changes were observed in the range of 2000–1200 cm^{-1}, as shown in Fig. 5b and c. The band at 1395 cm^{-1} attributed to symmetric R-COO^- stretching shifted to 1385 cm^{-1}. This result indicated that -COOH has been involved in Cd(II) adsorption, which was consistent with previous studies (Stathi et al., 2007; Du et al., 2017; Guo et al., 2017) and agreed with the XPS analysis discussed above. Interestingly, some new band at 1543 cm^{-1} was observed in the case of pH 9. These bands may indicate the N-containing groups were involved in Cd(II) adsorption, which was consistent with the XPS results.

For the Na-Mt-ALA$_{mix}$ at pH 5, the bands corresponding to R-COO^- symmetric deformation (1395 cm^{-1}) and CO-H bending (1431 cm^{-1}) shifted to 1385 cm^{-1} and 1412 cm^{-1}, respectively, after Cd(II) adsorption (Fig. 5c). These results suggested that carboxyl groups were involved in Cd(II) adsorption by forming carboxyl-Cd complexes. However, for Na-Mt-ALA$_{mix}$ at pH 7 and 9, except for the changes of carboxyl groups (i.e., R-COO^-), the band at 1619 cm^{-1} (band for the

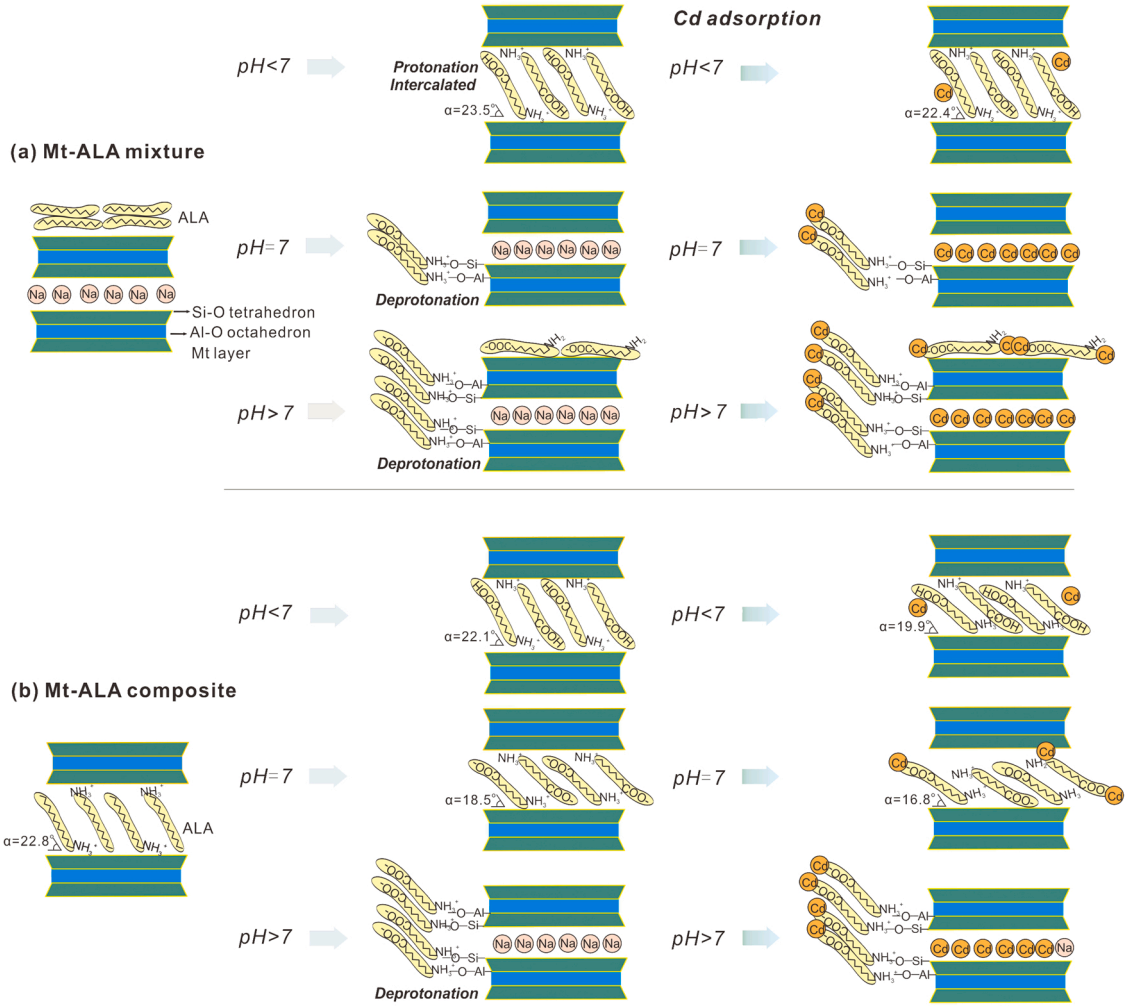

Fig. 6. The possible adsorption mechanisms of Cd(II) by Mt-ALA mixture and Mt-ALA composite at different pH. The tilting angles between ALA and silicate layers were calculated according to the size of ALA and stereochemical calculation based on Largaly et al. (2013), which could reflect the possible arrangement mode of OM in the interlayer space of Mt.

combination of O-H deformation and N-H bending (Yuan et al., 2013)) was shifted from 1643 cm^{-1} after Cd(II) adsorption. In addition, a new band at 1544 cm^{-1} (amide II band, Bu et al., 2019a; Yan et al., 2019) appeared after Cd(II) adsorption at pH 7 and 9, which showed the form of some amide-containing groups on the composite. These results indicated that the N-containing groups were involved in Cd(II) adsorption through forming the amino-Cd complex.

3.6. Metal uptake mechanisms and implications

The above results indicated that the presence of ALA changed the interlayer structure and surface properties of Mt at different pH, which affected the Cd(II) adsorption behavior (Fig. 6). It was believed that Mt has interlayer and edge (aluminol and silanol groups) adsorption sites for heavy metals (Brigatti et al., 2006; Fan et al., 2014). The former primarily arose from a structural charge originating from isomorphous substitutions within Mt structure. The latter was from a pH dependent charge related to proton adsorption/desorption reactions. Meanwhile, ALA was amphoteric, whose chemical structure in aqueous solution as a function of pH would be changed as some AAs molecules (i.e., glycine, Ramos and Huertas, 2013). Therefore, the interaction between Mt-ALA and Cd(II) at different pH was closely related to the changes of interlayer structure and surface charge induced by the variable charges of Mt (pH-dependent) and species of ALA (Kitadai et al., 2009).

For Na-Mt-ALA_{mix}, solid ALA cannot easily intercalate into the interlayers of clay in a dry state as described by XRD analysis. However, it's worth noting that when Na-Mt-ALA_{mix} was in aqueous solutions after acid and base treatment for 24 h before Cd adsorption , the reaction of ALA with interlayer strcuture of montmorillonite was greatly changed (Fig. 3). This thus leads to a significant difference in the adsorption of Cd between the MOA and the pure phase Mt. At acidic pH, the edge of the Mt was positively charged owing to the presence of surface $\equiv SOH_2^+$ groups. ALA was primarily present as zwitterion and cation $HALA^+$. Hence, positively charged cationic ALA can enter the interlayer space of Mt. Considering the concentration of ALA (200 mg/L) was higher than CEC of Mt, the positively charged amino groups would compete with Cd^{2+} for the adsorption sites of Mt. Under this circumstance, Cd(II) adsorption was primarily by binding carboxyl groups and $R\text{-}NH_3^+$ groups of the intercalated ALA and external ALA. Under neutral conditions, ALA was almost presented as zwitterion species, thus ALA was not found to enter the interlayer space described above. As pH increased from neutral to higher, the relative abundance of zwitterion species for ALA would decrease and anion ALA^- increase. For Mt, the charges in the edge sites were becoming negative for that Si-OH or Al-OH was deprotonated, resulting in the formation of $\equiv SO^-$ surface species (Stathi et al., 2007; Gu et al., 2010). This led to the amount of adsorbed ALA on edge increased and mainly located onto the external surface of Mt, which was implied by the d_{001} values as shown in Fig. 1. In this case, Cd(II) adsorption was by binding carboxyl and amino groups of the ALA, which was confirmed by XPS and FT-IR analyses. In addition, the interlayer

was able to attract the positively charged cationic Cd(II) or Cd-ALA complex, resulting in the d_{001} values increased. The possible Cd(II) adsorption mechanism of Mt-ALA mixture is summarized in Fig. 6a.

For Na-Mt-ALA_{inter}, ALA within the interlayer was not so much affected at an acidic condition because the interlayer distance remained constant (. The Cd(II) adsorption mechanism of Mt-ALA composite is illustrated in Fig. 6b. Under acidic conditions, Cd(II) adsorption sites were similar to that of Na-Mt-ALA_{mix}. Under neutral conditions, some of the interlayer ALA was released owing to the changes of ALA species (may from cationic $HALA^+$ to zwitterion). Cd(II) adsorption by Na-Mt-ALA_{inter} could be attributed to the binding of Cd^{2+} by the amino groups and carboxyl groups of the intercalated ALA. However, under basic conditions, ALA was mainly presented as an anion ALA^-. This led to almost all the ALA being desorbed from interlayer space and adsorbed on the edge sites of Mt. In this study, a significant improvement for Cd (II) adsorption could be observed compared with the Mt and Na-Mt-ALA_{mix} at pH 9. It can be attributed to that the higher pH environment diminished the "blocking effect" of interlayer organic matter and enhanced the formation of chelates (Zhu et al., 2019).

These results suggested that MOAs could adsorb Cd, and the adsorption capacity depended on various pH and types of MOAs. Clay mineral-AAs interactions in soils solution affect Cd adsorption. In particular, AAs can be protonated and intercalated into interlayer space under acidic conditions, which competed Cd(II) adsorption sites. But for interlayer MOAs, clay mineral-AAs-Cd(II) interactions are more likely to occur at high pH, exhibiting a larger Cd sink. The above findings seem to provide an insight into whether some clays serve as a metal sink once they encounter an environment where pH markedly increases or decreases. It was well known that differences in the chemistry of soils could cause variations in both the aqueous speciation of trace elements and clay surface properties (de Pablo et al., 2011). The clay surface properties variations can include clay surface site deprotonation and addition of surface functional groups as the complexation of OM or inorganic minerals (Landry et al., 2009). In this case, the interactions of the amphiprotic OM (i.e., amino acid) with clay minerals or heavy metal becomes more complicated in soils, especially for swelling clay minerals that provide considerable space for the heavy metals and some OM. The results of this study suggest that, when using clay minerals to immobilize toxic metals in contaminated soils, one should be considered checking the presence of AAs, as AAs can significantly affect the performance of clay minerals to the adsorption of heavy metals.

4. Conclusions

In this study, the adsorption mechanisms of Cd(II) by MOAs under different pH conditions were investigated. The results showed that the adsorption capacities of Cd(II) by MOAs were mainly dependent on the interlayer microstructure and species of ALA. Under acidic conditions, the interlayer of Mt was occupied by cationic $HALA^+$ that could compete with Cd(II) for adsorption sites, inhibiting the Cd(II) adsorption. In contrast, anion ALA^- was adsorbed on the surface of Mt under basic conditions, improving the affinity of MOAs for Cd(II). It's noteworthy that some interlayer ALA would be released out under neutral conditions, decreasing the "block effect" of cationic $HALA^+$ for Cd adsorption. In addition, the adsorption isotherm data of MOAs at acidic and basic conditions could be well fitted by the Langmuir isotherm and Freundlich isotherm, respectively, which was a contrast for Mt, indicating that the presence of ALA changed the adsorption mechanism of Cd(II) by MOAs. The results of XPS and FT-IR indicated that Cd(II) could react with the functional groups of ALA, forming organic complexes (e.g., -R-COOCd and R-NH_2Cd). These results revealed the interactions between ALA and clay minerals and highlighted the role of amphoteric OM in the adsorption of heavy metals in clay-based soils.

CRediT authorship contribution statement

Wenpo Xu: Investigation, Data curation, Formal analysis, Writing – original draft. **Chengshuai Liu**: Writing – review & editing, Project administration. **Jian-Ming Zhu**: Writing – review & editing. **Hongling Bu**: Investigation, Writing – review & editing, Formal analysis, Supervision. **Hui Tong**: Writing – review & editing. **Manjia Chen**: Writing – review & editing, Project administration, Supervision. **Decan Tan**: Editing. **Ting Gao**: Editing. **Yizhang Liu**: Editing.

Declaration of Competing Interest

The authors declare that they have no known competing financial interests or personal relationships that could have appeared to influence the work reported in this paper.

Acknowledgments

This work was financially supported by the National Key R & D Program of China (2020YFC1808500), the National Natural Science Foundation of China (41977288), the GDAS' Project of Science and Technology Development (2020GDASYL-20200102019 and 2019GDASYL-0102002–5), the Construction Project of Modern Agricultural Science and Technology Innovation Alliance of Guangdong Province, China (2021KJ112), and the Guangzhou Science and Technology Plan Project (202102020842). The authors thank Dr. Shengqiao Long, Jimei Zhou for their assistance with the sample preparation and mass spectrometry.

Appendix A. Supporting information

Supplementary data associated with this article can be found in the online version at doi:10.1016/j.ecoenv.2022.113509.

References

Brigatti, M.F., Galan, E., Theng, B.K.G., 2006. Structures and mineralogy of clay minerals. Dev. Clay Sci. 1, 19–86.
Brigatti, M.F., Malferrari, D., Medici, L., Poppi, L., 2003. Effect of amino acids on the retention of copper by beidellite. Environ. Eng. Sci. 20, 601–606.
Bu, H., Liu, D., Yuan, P., Zhou, X., Liu, H., Du, P., 2019a. Ethylene glycol monoethyl ether (EGME) adsorption by organic matter (OM)-clay complexes: Dependence on the OM Type. Appl. Clay Sci. 168, 340–347.
Bu, H., Yuan, P., Liu, H., Liu, D., Liu, J., He, H., Zhou, J., Song, H., Li, Z., 2017. Effects of complexation between organic matter (OM) and clay mineral on OM pyrolysis. Geochim. Cosmochim. Ac. 212, 1–15.
Bu, H., Yuan, P., Liu, H., Liu, D., Qin, Z., Zhong, X., Song, H., Li, Y., 2019b. Formation of macromolecules with peptide bonds via the thermal evolution of amino acids in the presence of montmorillonite: Insight into prebiotic geochemistry on the early Earth. Chem. Geol. 510, 72–83.
Chabani, M., Amrane, A., Bensmaili, A., 2006. Kinetic modelling of the adsorption of nitrates by ion exchange resin. Chem. Eng. J. 125, 111–117.
Das, S.K., Das, A.R., Guha, A.K., 2007. A study on the adsorption mechanism of mercury on Aspergillus versicolor biomass. Environ. Sci. Technol. 41, 8281–8287.
de Oliveira, L.H., Trigueiro, P., Rigaud, B., da Silva-Filho, E.C., Osajima, J.A., Fonseca, M.G., Lambert, J.-F., Georgelin, T., Jaber, M., 2021. When RNA meets montmorillonite: Influence of the pH and divalent cations. Appl. Clay Sci. 214, 106234.
de Pablo, L., Chávez, M.L., Abatal, M., 2011. Adsorption of heavy metals in acid to alkaline environments by montmorillonite and Ca-montmorillonite. Chem. Eng. J. 171 (3), 1276–1286.
Du, H., Chen, W., Cai, P., Rong, X., Dai, K., Peacock, C.L., Huang, Q., 2016a. Cd(II) sorption on montmorillonite-humic acid-bacteria composites. Sci. Rep. 6, 19499.
Du, H., Chen, W., Cai, P., Rong, X., Chen, C.R., Huang, Q., 2016b. Cadmium adsorption on bacteria-mineral mixtures: effect of naturally occurring ligands. Eur. J. Soil Sci. 67, 641–649.
Du, H., Chen, W., Cai, P., Rong, X., Feng, X., Huang, Q., 2016c. Competitive adsorption of Pb and Cd on bacteria-montmorillonite composite. Environ. Pollut. 218, 168–175.
Du, H., Qu, C., Liu, J., Chen, W., Cai, P., Shi, Z., Yu, X.Y., Huang, Q., 2017. Molecular investigation on the binding of Cd(II) by the binary mixtures of montmorillonite with two bacterial species. Environ. Pollut. 229, 871–878.
El Adraa, K., Georgelin, T., Lambert, J.-F., Jaber, F., Tielens, F., Jaber, M., 2017. Cysteine-montmorillonite composites for heavy metal cation complexation: a combined experimental and theoretical study. Chem. Eng. J. 314, 406–417.

Fan, Q.H., Tanaka, M., Tanaka, K., Sakaguchi, A., Takahashi, Y., 2014. An EXAFS study on the effects of natural organic matter and the expandability of clay minerals on cesium adsorption and mobility. Geochim. Cosmochim. Ac. 135, 49–65.
Gu, X., Evans, L.J., Barabash, S.J., 2010. Modeling the adsorption of Cd (II), Cu (II), Ni (II), Pb (II) and Zn (II) onto montmorillonite. Geochim. Cosmochim. Ac 74, 5718–5728.
Guo, Z., Zhang, X., Kang, Y., Zhang, J., 2017. Biomass-Derived Carbon Sorbents for Cd(II) Removal: Activation and Adsorption Mechanism. ACS Sustain. Chem. Eng. 5, 4103–4109.
Kitadai, N., Yokoyama, T., Nakashima, S., 2009. In situ ATR-IR investigation of L-lysine adsorption on montmorillonite. J. Colloid Interface Sci. 338, 395–401.
Lagaly, G., Ogawa, M., Dekany, I., 2013. Clay mineral-organic interactions. In: Bergaya, F., Lagaly, G. (Eds.), Handbook of Clay Science, Part A, second ed...,. Elsevier, Amsterdam, pp. 435–506.
Landry, C.J., Koretsky, C.M., Lund, T.J., Schaller, M., Das, S., 2009. Surface complexation modeling of Co(II) adsorption on mixtures of hydrous ferric oxide, quartz and kaolinite. Geochim. Cosmochim. Ac. 73, 3723–3737.
Liu, H., Yuan, P., Qin, Z., Liu, D., Tan, D., Zhu, J., He, H., 2013. Thermal degradation of organic matter in the interlayer clay-organic complex: a TG-FTIR study on a montmorillonite/12-aminolauric acid system. Appl. Clay Sci. 80–81, 398–406.
Liu, Y., Xiao, T., Zhu, Z., Ma, L., Li, H., Ning, Z., 2021. Geogenic pollution, fractionation and potential risks of Cd and Zn in soils from a mountainous region underlain by black shale. Sci. Total Environ. 760, 143426.
Ma, L., Zhu, J., Xi, Y., Zhu, R., He, H., Liang, X., Ayoko, G.A., 2015. Simultaneous adsorption of Cd(II) and phosphate on Al_{13} pillared montmorillonite. RSC Adv. 5, 77227–77234.
Ma, Y., Zhu, J., He, H., Yuan, P., Shen, W., Liu, D., 2010. Infrared investigation of organo-montmorillonites prepared from different surfactants. Spectrochim. Acta A 76 (2), 122–129.
Mo, X., Siebecker, M.G., Gou, W., Li, L., Li, W., 2021. A review of cadmium sorption mechanisms on soil mineral surfaces revealed from synchrotron-based X-ray absorption fine structure spectroscopy: Implications for soil remediation. Pedosphere 31, 11–27.
Mobasherpour, I., Salahi, E., Pazouki, M., 2012. Comparative of the removal of Pb^{2+}, Cd^{2+} and Ni^{2+} by nano crystallite hydroxyapatite from aqueous solutions: Adsorption isotherm study. Arab. J. Chem. 5, 439–446.
Naidu, R., Kookana, R.S., Sumner, M.E., Barter, R.D., Tiller, K.G., 1997. Cadmium sorption and transport in variable charge soils a review. J. Environ. Qual. 26, 602–617.
Nriagu, J.O., 1990. Global metal pollution: poisoning the biosphere? Environ. Sci. Policy Sust. Dev. 32, 7–33.
Parbhakar, A., Cuadros, J., Sephton, M.A., Dubbin, W., Coles, B.J., Weiss, D., 2007. Adsorption of L-lysine on montmorillonite. Colloids Surf. A Physicochem. Eng. Asp. 307, 142–149.
Ramos, M.E., Huertas, F.J., 2013. Adsorption of glycine on montmorillonite in aqueous solutions. Appl. Clay Sci. 80–81, 10–17.
Rothstein, D.E., 2010. Effects of amino-acid chemistry and soil properties on the behavior of free amino acids in acidic forest soils. Soil Biol. Biochem. 42 (10), 1743–1750.
Satarug, S., Baker, J.R., Urbenjapol, S., Haswell-Elkins, M., Reilly, P.E.B., Williams, D.J., Moore, M.R., 2003. A global perspective on cadmium pollution and toxicity in non-occupationally exposed population. Toxicol. Lett. 137, 65–83.
Stathi, P., Litina, K., Gournis, D., Giannopoulos, T.S., Deligiannakis, Y., 2007. Physicochemical study of novel organoclays as heavy metal ion adsorbents for environmental remediation. J. Colloid Interface Sci. 316, 298–309.
Teng, D., Zhang, B., Xu, G., Wang, B., Mao, K., Wang, J., Sun, J., Feng, X., Yang, Z., Zhang, H., 2020. Efficient removal of Cd(II) from aqueous solution by pinecone biochar: Sorption performance and governing mechanisms. Environ. Pollut. 265, 115001.
Theng, B.K.G., Churchman, G.J., Gates, W.P., Yuan, G., 2008. Organically modified clays for pollution uptake and environmental protection. In: Huang, Q., Huang, P.M., Violante, A. (Eds.), Soil Mineral-Microbe-Organic Interactions: Theories and Applications. Springer-Verlag, Berlin, pp. 145–174.
Van Riemsdijk, W.H., Koopal, L.K., Kinniburgh, D.G., Benedetti, M.F., Hiemstra, T., Weng, L., 2006. Modeling the Interactions between Humics, Ions, and Mineral Surfaces. Environ. Sci. Technol. 40, 7473–7480.
Xu, H., Zhu, S., Xia, M., Wang, F., 2021. Rapid and efficient removal of diclofenac sodium from aqueous solution via ternary core-shell CS@PANI@LDH composite: Experimental and adsorption mechanism study. J. Hazard. Mater. 402, 123815.
Xu, H., Zhu, S., Xia, M., Wang, F., Ju, X., 2022. Three-dimension hierarchical composite via in-situ growth of Zn/Al layered double hydroxide plates onto polyaniline-wrapped carbon sphere for efficient naproxen removal. J. Hazard. Mater. 423, 127192.
Yan, S., Cai, Y., Li, H., Song, S., Xia, L., 2019. Enhancement of cadmium adsorption by EPS-montmorillonite composites. Environ. Pollut. 252, 1509–1518.
Yang, L.P., Zhu, J., Wang, P., Zeng, J., Yang, Y.Z., Liu, Z.M., 2018. Effect of Cd on growth, physiological response, Cd subcellular distribution and chemical forms of Koelreuteria paniculata. Ecotoxicol. Environ. Saf. 160, 10–18.
Yuan, P., Liu, H., Liu, D., Tan, D., Yan, W., He, H., 2013. Role of the interlayer space of montmorillonite in hydrocarbon generation: an experimental study based on high temperature-pressure pyrolysis. Appl. Clay Sci. 75–76, 82–91.
Zhou, W., Ren, L., Zhu, L., 2017. Reducement of cadmium adsorption on clay minerals by the presence of dissolved organic matter from animal manure. Environ. Pollut. 223, 247–254.
Zhu, R., Chen, Q., Zhou, Q., Xi, Y., Zhu, J., He, H., 2016. Adsorbents based on montmorillonite for contaminant removal from water: A review. Appl. Clay Sci. 123, 239–258.
Zhu, S., Khan, M.A., Kameda, T., Xu, H., Wang, F., Xia, M., Yoshioka, T., 2022. New insights into the capture performance and mechanism of hazardous metals Cr^{3+} and Cd^{2+} onto an effective layered double hydroxide based material. J. Hazard. Mater. 426, 128062.
Zhu, S., Xia, M., Chu, Y., Khan, M.A., Lei, W., Wang, F., Muhmood, T., Wang, A., 2019. Adsorption and desorption of Pb(II) on L-lysine modified montmorillonite and the simulation of interlayer structure. Appl. Clay Sci. 169, 40–47.